

Geometric control of a quadrotor in wind with flow sensing and thrust constraints: Attitude and position control

William Craig^{*}, Derrick Yeo[†], and Derek A. Paley[‡]
University of Maryland, College Park, MD, 20742

Quadrotors show promise for a wide variety of outdoor missions, but struggle to fly reliably in windy conditions. This problem is partially addressed in this work by implementing custom flow probes on a quadrotor for flow-aware feedback control. The aerodynamic forces and moments resulting from wind interactions are modeled and incorporated into the quadrotor dynamics. Wind velocity data from the flow probes is fed back into a nonlinear feedback controller that guarantees stability under windy conditions and in the presence of thrust constraints. Experimental testing with motion capture in a gust-generation facility demonstrates the benefits of flow feedback for flight control in unsteady winds.

I. Nomenclature

A_f	=	quadrotor frontal area, m^2
C_D	=	quadrotor body drag coefficient
C_{l_α}	=	airfoil lift slope, $1/rad$
I_β	=	blade moment of inertia, kgm^2
J	=	quadrotor moment of inertia matrix, kgm^2
M_β	=	scaled aerodynamic moment on blade
N_b	=	number of blades per rotor
N_r	=	number of rotors
N_β	=	blade static moment, kgm
\mathbf{V}_∞	=	wind velocity, m/s
\mathbf{V}_{probe}	=	wind velocity measured by flow probe, m/s
\mathbf{X}_{probe}	=	flow probe position, m
c	=	blade chord, m
c_m	=	coefficient of thrust to torque, N/Nm
e	=	blade hinge offset, m
k_{λ_x}	=	Glauert longitudinal inflow gradient
ℓ	=	quadrotor cross beam length, m
m	=	quadrotor mass, kg
m_m	=	motor mass, kg
m_ℓ	=	cross beam mass, kg
r	=	displacement along the length of the blade, m
r'	=	non-dimensional displacement along the length of the blade
\bar{r}	=	rotor blade length, m
$\Delta\mathbf{V}_\infty$	=	velocity of wind relative to quadrotor, m/s
Ψ	=	configuration error function
α_{eff}	=	effective angle of attack, rad
α_{geo}	=	geometric angle of attack, rad
α_{ind}	=	induced angle of attack, rad
β	=	blade flap angle, rad

^{*}Graduate Research Assistant, Department of Aerospace Engineering and Institute for Systems Research, wscraig@umd.edu, AIAA Student Member.

[†]Assistant Clinical Professor, Department of Aerospace Engineering, dyeo@umd.edu, AIAA Member.

[‡]Willis H. Young Jr. Professor of Aerospace Engineering Education, Department of Aerospace Engineering and Institute for Systems Research, dpaley@umd.edu, AIAA Associate Fellow.

β_0	=	blade coning angle, <i>rad</i>
β_{1c}	=	longitudinal blade flapping angle, <i>rad</i>
β_{1s}	=	lateral blade flapping angle, <i>rad</i>
β_{max}	=	maximum blade flap angle, <i>rad</i>
γ	=	Lock number
θ_0	=	blade root angle of attack, <i>rad</i>
θ_{tw}	=	linear blade twist, <i>rad</i>
λ_0	=	average inflow ratio
λ_i	=	linear inflow ratio
μ	=	quadrotor advance ratio
ν	=	quadrotor input moment, <i>Nm</i>
ν_β	=	blade scaled natural frequency
ρ	=	density of air, <i>kg/m³</i>
ϕ_D	=	blade-flapping azimuthal phase delay, <i>rad</i>
ψ_β	=	blade azimuth angle, <i>rad</i>
ω_j	=	angular speed of rotor <i>j</i> , <i>rad/s</i>

II. Introduction

QUADROTOR unmanned aerial systems (UAS) are becoming powerful tools for both commercial and military applications. Their utility has already been demonstrated in missions such as surveying farmland and aiding in natural disasters [1, 2]. As they continue to prove their effectiveness in relatively predictable environments, work is ongoing to extend their mission capability, including sensing and perception for unknown environments [3–5], aerobatic behavior [6, 7], hardware failures [8], and transportation of suspended loads [9, 10]. A lingering challenge is flight stability in wind gusts. In this work, we use a model of the aerodynamic interaction between the propellers and wind paired with onboard flow sensing and feedback control to improve the stability of quadrotors in unsteady winds, with the long-term goal of allowing for reliable outdoor flight in windy conditions.

The aerodynamic interaction of quadrotor propellers with wind is modeled using the blade-flapping phenomena more commonly associated with full-size single-main-rotor helicopters [11]. When a helicopter flies forward, one side of the rotor advances into the oncoming free-stream velocity, while the other side retreats from the free-stream velocity, which leads to an increase in dynamic pressure and lift on the advancing side and a decrease in dynamic pressure and lift on the retreating side. The dissymmetry of lift yields a moment on the rotor blades that causes the blades to flap out of the plane of the hub, tilting the rotor plane and imparting a moment on the hub. Many quadrotors ignore the blade-flapping phenomena while maintaining acceptable performance [6, 7, 12, 13]. However, to improve performance in unsteady winds by use of feedback control we seek an accurate model of the aerodynamic interactions, allowing the controller to address the wind gusts directly rather than using an uncertainty block characteristic of robust control [14].

The feedback controller described here relies on onboard flow measurements from multi-hole probes to estimate the aerodynamic forces and moments on the quadrotor. By using flow measurements as well as inertial sensing, the controller can react to the wind before the resulting moment has propagated to the quadrotor’s dynamics, which yields benefits compared to relying on inertial sensing alone. Work validating the benefit of flow feedback was performed in [15] for a one degree-of-freedom pitching test stand, and in [16] for a three degree-of-freedom attitude test stand. The flow sensor package consists of fore and aft, and left and right facing probe pairs connected to a microcontroller unit through flexible tubing [4]. The microcontroller measures pairwise differential pressure, and transmits a digital signal to the flight controller corresponding to the horizontal wind components in the body frame.

The specific flight controller on which we build our flow-feedback design uses feedback linearization on the geometric Lie group $SE(3)$ following [17], with the addition of thrust constraints. Compared to other quadrotor control approaches, such as PID [18, 19], robust [14, 20], adaptive [7, 21], and optimal [22] control, feedback linearization allows the controller to cancel the aerodynamic terms directly. Developing the controller on $SE(3)$, which is a compact set representing the configuration space of the orientation and position of a rigid body, avoids the singularities associated with Euler angles and allows for potentially global solutions.

In order to establish stability guarantees for the feedback-linearization controller, we require that the thrust does not saturate. Cao and Lynch [18] and Roza and Maggiore [23] approach thrust saturation using the nested saturation method from Teel [24], which is designed to address saturation in the case of a chain of integrators. Cao and Lynch [18] bound the roll and pitch angles of the system as well as the thrust by placing limits on system inputs, whereas Roza and

Maggiore [23] place the bound on thrust only. Cutler and How [19] address saturation by choosing a trajectory that keeps the system states within the bounds required to avoid thrust saturation. This paper uses the method of Pappas et al. [25] to bound the thrust on the system in order to guarantee stability when the cost of feedback linearization does not saturate the thrust.

The contributions of this paper are (1) a nonlinear, feedback-linearizing attitude and position controller on $SE(3)$ using flow sensing and accounting for saturated thrust inputs; and (2) an experimental demonstration of the benefit of flow probes on a quadrotor, including an assessment of the relative merits of adding flow sensing to the vehicle controller versus using inertial feedback alone. This paper extends the three degree-of-freedom attitude-only control in [16] to a six degree-of-freedom free-flight quadrotor.

The outline of the paper is as follows. Section III details the six degree-of-freedom rigid-body dynamics of the quadrotor vehicle, the blade-flapping dynamics resulting from aerodynamic interactions between the propellers and wind, and the inner-loop attitude controller. Section IV describes the outer-loop position controller and shows exponential stability of the complete system. Section V describes the experimental system and shows results from a six degree-of-freedom quadrotor subject to a series of gusts. Section VI summarizes the paper and discusses ongoing work.

III. Quadrotor Dynamics in Wind

A. Rigid-Body Dynamics

This work investigates attitude and position control of a quadrotor in six degree-of-freedom (DOF) flight. Define inertial reference frame $\mathcal{I} \triangleq (O, \mathbf{e}_1, \mathbf{e}_2, \mathbf{e}_3)$ in an east, north, up orientation and body reference frame $\mathcal{B} \triangleq (O', \mathbf{b}_1, \mathbf{b}_2, \mathbf{b}_3)$ in a forward, left, up orientation. Let the position of the center of mass O' of the quadrotor relative to an inertial reference frame be given by $\mathbf{x} \in \mathbb{R}^3$, and let the orientation of the quadrotor relative to the inertial frame be represented by the rotation matrix $R \in SO(3)$. The full system state of the quadrotor is represented by $\mathbf{x} \times R \in SE(3)$. The translational velocity of the quadrotor relative to the inertial frame is \mathbf{v} , and the angular velocity of the quadrotor relative to the inertial frame is $\boldsymbol{\Omega} = [p, q, r]^T$. We use bold capital letter notation for vectors in body frame components, lowercase bold letters for vectors in inertial components, a \mathcal{B} superscript for a body-frame derivative, and no superscript to indicate inertial-frame derivatives. Using rigid-body kinematics and Euler's laws, the translational and rotational dynamics are

$$\begin{aligned} \dot{\mathbf{x}} &= \mathbf{v} \\ m\dot{\mathbf{v}} &= -mg\mathbf{e}_3 + \mathbf{f}_{thrust} + \mathbf{f}_{aero} \\ \dot{R} &= R\hat{\boldsymbol{\Omega}} \\ J\dot{\boldsymbol{\Omega}} &= -\hat{\boldsymbol{\Omega}}J\boldsymbol{\Omega} + \mathbf{M}_{thrust} + \mathbf{M}_{aero}, \end{aligned} \tag{1}$$

where m is the mass of the quadrotor, g is the gravitational force, $\mathbf{f}_{thrust} = f_{thrust}\mathbf{b}_3$ is the total thrust generated by the vehicle, and \mathbf{f}_{aero} is the aerodynamic drag force on the vehicle from both the propellers' induced drag and the drag on the body. J is the moment of inertia matrix, which is diagonal due to the symmetry of the quadrotor. Moment \mathbf{M}_{thrust} is due to propeller thrusts and \mathbf{M}_{aero} is the aerodynamic moment due to interaction between the rotors and the wind. (The wedge operator \wedge converts a vector in \mathbb{R}^3 to a 3×3 skew symmetric matrix, which can also be used to represent a cross product, such that for any vectors \mathbf{x} and \mathbf{y} in \mathbb{R}^3 , $\hat{\mathbf{x}}\mathbf{y} = \mathbf{x} \times \mathbf{y}$. The vee operator \vee transforms a skew-symmetric matrix to a vector in \mathbb{R}^3 .)

The quadrotor vehicle is modeled as two perpendicular uniform beams of length ℓ attached at their centers to create four arms, with one rotor located at the end of each arm, as in Fig. 1. Rotors are located at position $d\mathbf{b}_3$ above each arm, where $d \ll \ell/2$. The moment of inertia is $J = \text{diag}\{m_\ell\ell^2/12 + 2m_m\ell^2, m_\ell\ell^2/12 + 2m_m\ell^2, m_\ell\ell^2/6 + 4m_m\ell^2\}$, where m_ℓ is the mass of each cross beam of the quadrotor, ℓ is the length of each cross beam, and m_m is the mass of each motor. Rotors are assumed to spin about the \mathbf{b}_3 axis, with rotation directions shown in Fig. 1. This choice of rotor rotational directions result in a net zero torque in the \mathbf{b}_3 direction under nominal conditions with each rotor operating at the same speed and no outside aerodynamic forces.

Thrust forces and moments on the vehicle are a result of the spinning rotors, each of which produces a thrust and a corresponding torque in the direction opposite its rotation. The blades are set up in counter-rotating pairs, leading to cancellation of the component of the aerodynamic moment \mathbf{M}_{aero} along the \mathbf{u}_1 -axis, where \mathbf{u}_1 describes the direction of the wind in the plane of the hub and $\mathbf{u}_3 = \mathbf{b}_3$. The wind components in the body frame are measured by a multi-hole probe [4], which allows us to find the moment on the rotors from the identification of the phase delay ϕ_D and the magnitude β_{\max} of the angle of maximum flapping.

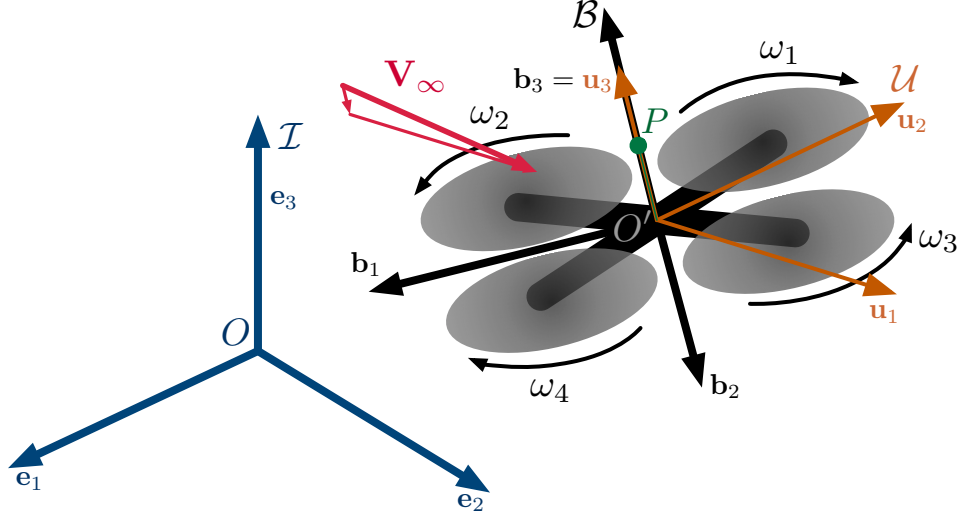


Fig. 1 Quadrotor reference frames: \mathcal{I} is the inertial frame, \mathcal{B} is the body frame, \mathcal{U} is the wind frame. The flow probe is situated at point P and \mathbf{u}_1 is aligned with the horizontal component of the wind \mathbf{V}_∞

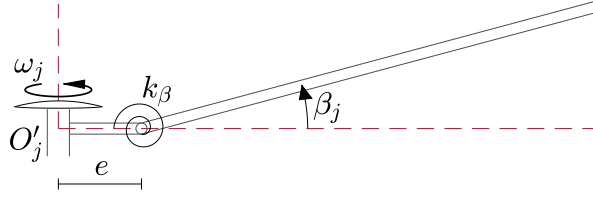


Fig. 2 Blade-flapping model [11], where O'_j is the position of the j^{th} hub, β_j is the flap angle of blade j , k_β is the flap spring, e is the hinge offset, and ω_j is the rotational speed of rotor j

The multi-hole probe P measures the wind at position \mathbf{X}_{probe} above the quadrotor's center of mass O' to reduce the effect of the vehicle drag and propeller inflow, so the quadrotor's rotation must be accounted for when determining the wind velocity at O' . The vector measured by the flow probe is \mathbf{V}_{probe} , the inertial wind velocity in body-frame components is \mathbf{V}_∞ , the quadrotor translational velocity in body components is \mathbf{V} , and the contribution of the quadrotor rotational velocity is $\hat{\boldsymbol{\Omega}}\mathbf{X}_{probe}$. The value measured by the probe is

$$\mathbf{V}_{probe} = \mathbf{V}_\infty - \mathbf{V} - \hat{\boldsymbol{\Omega}}\mathbf{X}_{probe}. \quad (2)$$

Let $\Delta\mathbf{V}_\infty = \mathbf{V}_\infty - \mathbf{V} = \mathbf{V}_{probe} + \hat{\boldsymbol{\Omega}}\mathbf{X}_{probe}$ be the velocity of wind experienced over the center of mass of the quadrotor. Note, Eq. (2) assumes the probe measures all three vector components of the wind in the body frame; in the experimental testbed, we only measure the two horizontal components.

B. Blade-flapping Dynamics

We model the aerodynamic moment on the quadrotor as a result of the blade-flapping phenomena in rotorcraft, which occurs due to uneven lift on the advancing and retreating blades as the vehicle flies forward and/or is subject to wind [11]. We follow the single-propeller analysis in [26] to develop the aerodynamic moment \mathbf{M}_{aero} acting on the quadrotor, derived in [16].

We define a number of additional variables to mathematically describe blade flapping. Let β be the flap angle of the blade away from the plane of the hub, v_β be the scaled natural frequency of the propeller blade, and consider the Lock number γ , which is the ratio of aerodynamic to inertial forces on the blade. Define M_β as the moment resulting from the

aerodynamic interaction between the propeller and the wind. Define ω as the propeller angular velocity, N_β as the static moment of the blade, and I_β as the moment of inertia of the blade. Blade flapping is described by the equation [11]

$$\beta^{**} + v_\beta^2 \beta = \gamma M_\beta - \frac{g N_\beta}{\omega^2 I_\beta}, \quad (3)$$

where $*$ denotes differentiation with respect to blade azimuth $\psi_\beta = \omega t$ such that $\dot{\beta} \triangleq \omega \beta^*$, following [11].

The moment M_β is derived using the lift and drag forces on the blade, and results in an expression that depends on the geometric blade parameters θ_0 and θ_{tw} , which are the root angle of attack and twist of the blade, respectively; the hinge offset of the blade e shown in Fig. 2; and the inflow conditions, described by the average inflow through the propeller λ_0 and the total linear inflow over the propeller $\lambda_i = \lambda_0(1 + k_{\lambda_x} r' \cos(\psi_\beta))$, where k_{λ_x} is the slope of the inflow and depends on the wind speed, r' is the non-dimensional length along the propeller blade, and ψ_β is the azimuth angle of the blade around the hub. Equation (3) is solved by matching first harmonic terms on each side, i.e., $\beta(\psi_\beta) = \beta_0 + \beta_{1c} \cos(\psi_\beta) + \beta_{1s} \sin(\psi_\beta)$ [26]. To predict the aerodynamic moment \mathbf{M}_{aero} , we need to solve for the maximum flapping amplitude and where it occurs in the azimuth, which can be described by $\beta_{\max} = \sqrt{\beta_{1c}^2 + \beta_{1s}^2}$ and phase delay $\phi_D = \tan^{-1}(\beta_{1s}/\beta_{1c}) - \pi/2$ [26].

In the complete development, β_{1s} and β_{1c} are implicit equations, so we make simplifications for tractability. We find that for our parameters, the hinge offset e and the implicit multipliers contribute little to the overall flapping behavior and, when ignored, result in much simpler, explicit equations that depend only on inflow, forward speed, and blade parameters [26]:

$$\beta_{1c} \approx \frac{-\gamma}{8(v_\beta^2 - 1)} \lambda_0 k_{\lambda_x} \quad (4)$$

and

$$\beta_{1s} \approx \frac{\mu \gamma}{4(v_\beta^2 - 1)} \left(\frac{4}{3} \theta_0 + \theta_{tw} - \lambda_0 \right). \quad (5)$$

The overall aerodynamic moment on the hub \mathbf{M}_{aero} depends on the maximum flap angle β_{\max} for the spring force at the blade hinge as well as the force resulting from the hinge offset, and also considers the pitching moment of the blade itself [26]. However, we ignore the hinge offset and blade pitching moment contributions because the spring force provides the majority of the moment at the hub. When solving for the total aerodynamic moment on the quadrotor, counter-rotating pairs cancel the \mathbf{u}_1 component to yield the moment used for attitude control [16]

$$\mathbf{M}_{aero} = [4k_\beta \beta_{\max} S_{\phi_D} \mathbf{u}_2 \cdot \mathbf{b}_1, 4k_\beta \beta_{\max} S_{\phi_D} \mathbf{u}_2 \cdot \mathbf{b}_2, 0]^T, \quad (6)$$

where $k_\beta = 3$ for the Gemfan 5030 rotors used here [26].

C. Attitude Control Design on SO(3)

This work leverages the inner-loop attitude control design in [16]. The desired attitude is represented as a rotation matrix R_d , and is applied in the attitude controller using the configuration error function [27]

$$\Psi(R, R_d) = \frac{1}{2} \text{tr}(I - R_d^T R), \quad (7)$$

which is locally positive definite when the angle between R and R_d , defined by $\theta_R = \arccos((\text{tr}[R_d^T R] - 1)/2)$, is less than π [17], which occurs almost globally. The attitude tracking error \mathbf{e}_R is [17]

$$\mathbf{e}_R = \frac{1}{2} (R_d^T R - R^T R_d)^\vee, \quad (8)$$

which is derived from the configuration error function. The angular-velocity tracking error is [17]

$$\mathbf{e}_\Omega = \Omega - R^T R_d \Omega_d. \quad (9)$$

Note $d(R_d^T R)/dt = (R_d^T R) \hat{\mathbf{e}}_\Omega$, when compared to (1), shows \mathbf{e}_Ω is to $R_d^T R$ as Ω is to R .

In order to minimize the rate and attitude errors, we stabilize our system using the thrust moment in Eq. (11). The 6-DOF quadrotor is underactuated, so we specify inputs corresponding to the overall thrust and the roll, pitch, and yaw moments. This relationship can be inverted to yield

$$\begin{aligned}
T_1 &= T_0 + \frac{1}{4}(-v_1 + v_2 + v_3) \\
T_2 &= T_0 + \frac{1}{4}(-v_1 - v_2 - v_3) \\
T_3 &= T_0 + \frac{1}{4}(v_1 + v_2 - v_3) \\
T_4 &= T_0 + \frac{1}{4}(v_1 - v_2 + v_3).
\end{aligned} \tag{10}$$

Based on the position and rotation of each motor, the thrust moment on the quadrotor is

$$\mathbf{M}_{thrust} = \begin{bmatrix} \frac{\ell\sqrt{2}}{4}(-T_1 - T_2 + T_3 + T_4) \\ \frac{\ell\sqrt{2}}{4}(T_1 - T_2 + T_3 - T_4) \\ c_m(T_1 - T_2 - T_3 + T_4) \end{bmatrix}, \tag{11}$$

where c_m is a coefficient relating the thrust produced to the torque of the motor, found empirically to be approximately 0.0085 Nm/N for the testbed described in Section V. Thus, from Eq. (10),

$$\mathbf{M}_{thrust} = \begin{bmatrix} \frac{\ell\sqrt{2}}{4}v_1, \frac{\ell\sqrt{2}}{4}v_2, c_mv_3 \end{bmatrix}^T. \tag{12}$$

Define $H = \text{diag}\{\ell\sqrt{2}/4, \ell\sqrt{2}/4, c_m\}$ and $\mathbf{v} = [v_1, v_2, v_3]^T$, then choose [28]

$$\mathbf{v} = H^{-1}J[-k_R\mathbf{e}_R - k_\Omega\mathbf{e}_\Omega - J^{-1}(-\hat{\Omega}J\Omega + \mathbf{M}_{aero}) - \hat{\Omega}R^T R_d\Omega_d + R^T R_d\dot{\Omega}_d], \tag{13}$$

yielding the thrust moment [16]

$$\mathbf{M}_{thrust} = -Jk_R\mathbf{e}_R - Jk_\Omega\mathbf{e}_\Omega + \hat{\Omega}J\Omega - \mathbf{M}_{aero} + J(-\hat{\Omega}R^T R_d\Omega_d + R^T R_d\dot{\Omega}_d). \tag{14}$$

When Eq. (14) is inserted in Eq. (9), the attitude error dynamics become [28]

$$\begin{aligned}
\dot{\mathbf{e}}_R &= \frac{1}{2}(\text{tr}\{R^T R_d\}I - R^T R_d)\mathbf{e}_\Omega, \\
\dot{\mathbf{e}}_\Omega &= -k_R\mathbf{e}_R - k_\Omega\mathbf{e}_\Omega,
\end{aligned} \tag{15}$$

which are exponentially stable according to Proposition 1 in [16]. Furthermore, we employ a variable-gain method [16] to prevent motor saturation and maintain stability guarantees: if control authority exists after feedback linearization, choose gain coefficient $0 < k_{mod} \leq 1$ to scale the stabilizing inputs uniformly such that motor limits are not exceeded and the direction of the stabilizing moment is preserved.

IV. Position Control Design on SE(3)

By representing the kinematics using rotation matrices in the Lie group $SE(3)$, we design a flow-aware position and attitude controller that achieves nearly global stabilization while avoiding singularities associated with Euler angles. The controller follows [17] using a cascaded inner-loop, outer-loop architecture, where the outer loop solves for position errors and prescribes the direction of \mathbf{b}_3 as well as the total thrust \mathbf{f}_{thrust} . The desired \mathbf{b}_1 direction is prescribed independently of \mathbf{f}_{thrust} and \mathbf{b}_3 . The thrust force and axis directions are transmitted to the inner loop, where desired roll and pitch angles are determined based on \mathbf{b}_{3_d} , and desired yaw angle is determined by \mathbf{b}_{1_d} . Attitude control development differs from previous work [16] in that the average thrust T_0 is no longer constant, which may be incorporated in the analysis of [16] without additional modification.

The desired attitude R_d driving the inner-loop controller is developed based on the position and heading error of the quadrotor. Tracking errors are defined as [17]

$$\begin{aligned}
\mathbf{e}_x &= \mathbf{x} - \mathbf{x}_d, \\
\mathbf{e}_v &= \mathbf{v} - \mathbf{v}_d,
\end{aligned} \tag{16}$$

where \mathbf{x}_d and \mathbf{v}_d are the desired position and velocity, respectively. For a given smooth tracking command $\mathbf{x}_d(t)$, and positive constants k_x and k_v , define [17]

$$\mathbf{b}_{3d} = \frac{-k_x \mathbf{e}_x - k_v \mathbf{e}_v + m \mathbf{g} \mathbf{e}_3 + m \ddot{\mathbf{x}}_d - \mathbf{f}_{aero}}{\| -k_x \mathbf{e}_x - k_v \mathbf{e}_v + m \mathbf{g} \mathbf{e}_3 + m \ddot{\mathbf{x}}_d - \mathbf{f}_{aero} \|}, \quad (17)$$

where we assume $\| -k_x \mathbf{e}_x - k_v \mathbf{e}_v + m \mathbf{g} \mathbf{e}_3 + m \ddot{\mathbf{x}}_d - \mathbf{f}_{aero} \| \neq 0$, and include the aerodynamic drag term \mathbf{f}_{aero} as follows.

The drag force results from bluff body drag on the quadrotor as well as induced drag from the propellers such that $\mathbf{f}_{aero} = \mathbf{f}_{bluff} + \mathbf{f}_{ind}$. Define A_f as the frontal area of the quadrotor and C_D as the drag coefficient of the quadrotor. Bluff body drag is modeled as

$$\mathbf{f}_{bluff} = \frac{1}{2} \rho \|\Delta \mathbf{v}_\infty\| A_f C_D \Delta \mathbf{v}_\infty, \quad (18)$$

where $\Delta \mathbf{v}_\infty = R(\mathbf{V}_{probe} + \hat{\Omega} \mathbf{X}_{probe})$. Induced drag results from the lift force and induced angle of attack. Let $\alpha_{ind} = \arctan(\lambda_0/0.75)$ denote the induced angle of attack (using for simplicity the average angle, rather than integrating across the blade), which results from the velocity of the wind relative to the rotating blade; $\alpha_{eff} = \alpha_{geo} - \alpha_{ind}$ be the effective angle of attack; and α_{geo} be the geometric angle of attack resulting from the blade pitch relative to the plane of the hub. Define N_r as the number of rotors on the vehicle, N_b as the number of blades per rotor, and \bar{r} as the length of the rotor blade. Induced drag is

$$\mathbf{f}_{ind} = N_r \frac{N_b}{2\pi} \int_0^{2\pi} \int_0^{\bar{r}} \frac{1}{2} \rho (\omega r + S_{\psi_\beta} (\Delta \mathbf{v}_\infty \cdot \mathbf{u}_1))^2 c C_{\ell_\alpha} \alpha_{eff} S_{\alpha_{ind}} S_{\psi_\beta} dr d\psi_\beta \mathbf{u}_1, \quad (19)$$

which is then integrated along the length of the blade and around one rotor revolution. To avoid the multivariable integration, we simplify the induced angle of attack term α_{ind} in Eq. (19) by assuming uniform inflow, using the mean velocity of the blade, neglecting the change in velocity due to wind, and assuming the angle is small, such that $\alpha_{ind} = 2\lambda_0$. Additionally, we assume a constant effective angle of attack $\alpha_{eff} = \theta_0 + (3/4)\theta_{tw} - \alpha_{ind}$, which yields the following:

$$\mathbf{f}_{ind} \approx N_r \frac{N_b}{4} \rho c C_{\ell_\alpha} \alpha_{eff} S_{\alpha_{ind}} \omega \bar{r}^2 (\Delta \mathbf{v}_\infty \cdot \mathbf{u}_1) \mathbf{u}_1. \quad (20)$$

The drag force is incorporated in \mathbf{b}_{3d} , and thrust force is correspondingly chosen as

$$\mathbf{f}_{thrust} = (-k_x \mathbf{e}_x - k_v \mathbf{e}_v + m \mathbf{g} \mathbf{e}_3 + m \ddot{\mathbf{x}}_d - \mathbf{f}_{aero}) \cdot \mathbf{b}_3. \quad (21)$$

We also prescribe the desired heading \mathbf{b}_{1d} in the outer loop, and assume that \mathbf{b}_{1d} is not parallel to \mathbf{b}_{3d} . Then the desired attitude of the quadrotor transmitted to the inner-loop controller is $R_d = [\mathbf{b}_{2d} \times \mathbf{b}_{3d}, \mathbf{b}_{2d}, \mathbf{b}_{3d}] \in SO(3)$, where $\mathbf{b}_{2d} = (\mathbf{b}_{3d} \times \mathbf{b}_{1d}) / \|\mathbf{b}_{3d} \times \mathbf{b}_{1d}\|$. Additionally, we assume $\|m \mathbf{g} \mathbf{e}_3 + m \ddot{\mathbf{x}}_d\| < B$ for a given positive constant B . Then, the complete error dynamics of the system are

$$\begin{aligned} \dot{\mathbf{e}}_R &= \frac{1}{2} \left(\text{tr} \{ R^T R_d \} I - R^T R_d \right) \mathbf{e}_\Omega, \\ \dot{\mathbf{e}}_\Omega &= J^{-1} \left(-\hat{\Omega} J \Omega + \mathbf{M}_{thrust} + \mathbf{M}_{aero} \right) + \hat{\Omega} R^T R_d \Omega_d - R^T R_d \dot{\Omega}_d, \\ m \dot{\mathbf{e}}_x &= m \dot{\mathbf{x}} - m \dot{\mathbf{x}}_d = m \mathbf{v} - m \mathbf{v}_d \\ m \dot{\mathbf{v}} &= m \ddot{\mathbf{x}} - m \ddot{\mathbf{x}}_d = -m \mathbf{g} \mathbf{e}_3 + \mathbf{f}_{thrust} + \mathbf{f}_{aero} \end{aligned} \quad (22)$$

The stability of the dynamics in Eq. (22) relies on the convergence of the attitude dynamics in order to ensure that \mathbf{b}_3 follows \mathbf{b}_{3d} . Almost global exponential stability of the attitude dynamics is shown in [16] using the moment input in Eq. (14). Furthermore, for stability of the complete dynamics we require the initial attitude error to be less than $\pi/2$ [17], corresponding to the configuration error function Ψ less than 1. Applying the control force \mathbf{f}_{thrust} and moment \mathbf{M}_{thrust} defined in Eqs. (21) and (14), the dynamics in Eq. (22) are exponentially stable according to Proposition 2 in [17], with the region of attraction characterized by $\Psi(R(0), R_d(0)) \leq \psi_1 < 1$, where ψ_1 is a constant. Furthermore, although Proposition 2 in [17] requires that the initial attitude error be less than $\pi/2$, the attitude error function Ψ is guaranteed to exponentially decrease [16], and will therefore enter the region of attraction in a finite time, by which almost global exponential attractiveness of the complete dynamics is shown in Proposition 3 of [17].

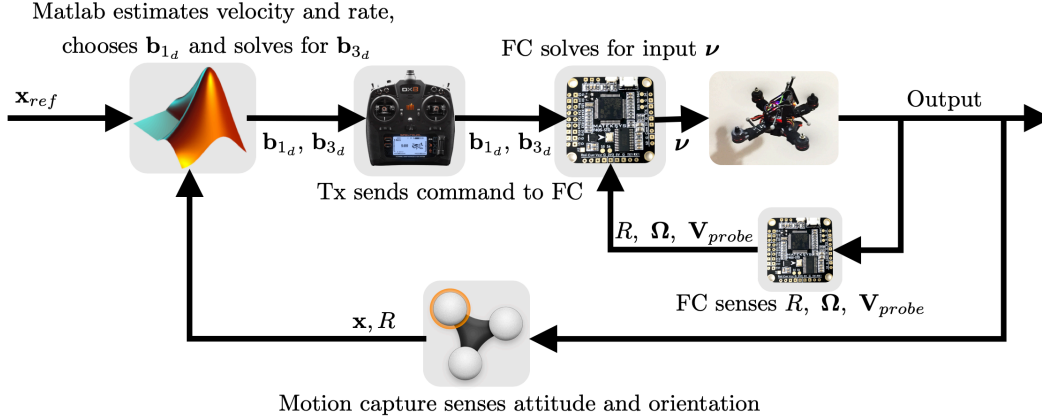


Fig. 3 Block diagram of experimental control loop, showing communication between motion capture, Matlab, transmitter (Tx) and flight controller (FC)

V. Closed-Loop Experimental Results in Wind Gusts

A. Quadrotor Testbed

Performance of the developed controller was tested experimentally with the quadrotor in Fig. 4b, using motion capture feedback for position and heading control, and onboard flight-controller sensing for inner-loop attitude control. The quadrotor is a 210 mm carbon fiber frame with a Matek F405 STD flight controller and Matek FCHUB-6S power distribution board. Gemfan 5030 propellers are mounted to EMAX RS-2205 motors that are controlled by EMAX Lightning 20A ESCs. The quadrotor runs Cleanflight open-source software that has been modified to support flow measurement feedback and run the feedback-linearization controller described above. The flow instrumentation utilizes custom-built pressure probes, highlighted in Fig. 4b, that provide information through differential-pressure measurements to sense wind speeds up to 8 m/s [4]. Data from the quadrotor is collected on a micro SD card using Cleanflight’s Blackbox feature at a rate of 250 Hz.

Position and attitude data are collected in an OptiTrack motion capture facility and streamed to the outer-loop controller running in Matlab as shown in Fig. 3. Errors, thrust, and desired body axes are computed and passed to the flight controller through the trainer port of an RC transmitter, where the custom Cleanflight software integrates flow measurements to solve for the final desired axes and produce the required thrust at each motor. In our experiments, we cannot directly control thrust, as was assumed in the controller design, so we use a linear fit relating the PWM value from the transmitter to the force output from the propellers [16] with a slope of 0.021 N/PWM.

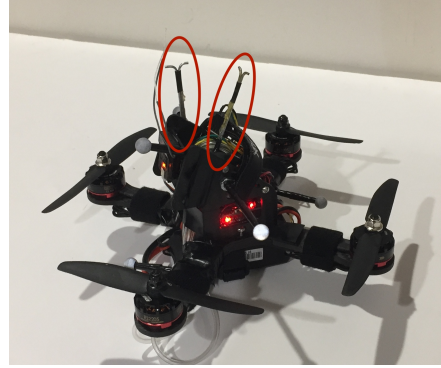
Gust rejection testing is performed using a custom gust-generator system, shown in Fig. 4a, consisting of a set of Dyson fans behind remotely actuated blinds controlled through Labview using an Arduino. Baseline wind speeds are established prior to flight using a separate Testo 405i hot-wire anemometer, then tests are initialized with the quadrotor facing the fans such that \mathbf{e}_1 aligns with \mathbf{b}_1 , with $\Delta \mathbf{V}_\infty$ along $-\mathbf{e}_1$. After initialization, the quadrotor is flown to a specific position where it is commanded to hold station, then the blinds are opened and closed in a square-wave pattern to produce gusts.

B. Experimental Results

We experimentally compare three inner-loop control approaches: an attitude controller on $SO(3)$ with flow feedback, the same controller without flow feedback, and the PID controller standard in the Cleanflight software, which also lacks flow feedback. All approaches use the same outer-loop position control in Section IV, and the inner-loop for each controller was tuned by hand to achieve a fast response while maintaining stability. Tests in Figs. 5 and 7 are subjected to a 4 m/s gust in a square-wave pattern with a period of 10 seconds, and tests in Figs. 6 and 8 show gusts at the same speed with a period of 4 seconds. Figures 5 and 6 show the time series \mathbf{e}_1 error against the wind speeds measured onboard by the fore-aft flow probe. Figures 7 and 8 show the position of the vehicle from an overhead view in the $\mathbf{e}_1 - \mathbf{e}_2$ plane on the left, and a side view in the $\mathbf{e}_1 - \mathbf{e}_3$ plane on the right, together showing the full three-dimensional response of the quadrotor to wind.



(a) Gust generation system consists of a set of eight Dyson fans behind remotely operated blinds



(b) Experimental quadrotor vehicle with flow probes circled in red

Fig. 4 Experimental gust generation system and quadrotor

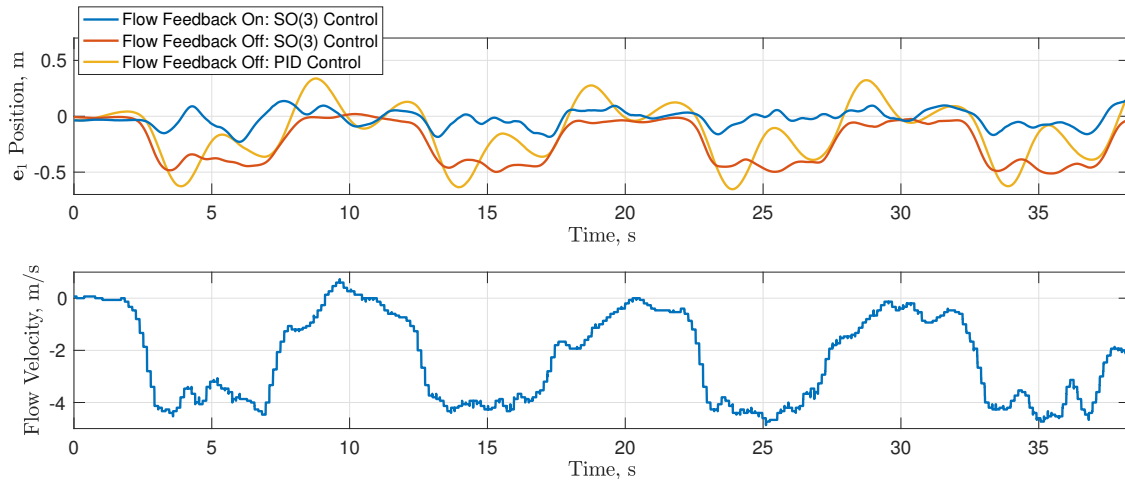


Fig. 5 Experimental quadrotor e_1 position error in response to 5 s duration 4 m/s gusts in the $-e_1$ direction. All three controllers use the same outer-loop control, and flow velocity is measured onboard using a custom flow probe.

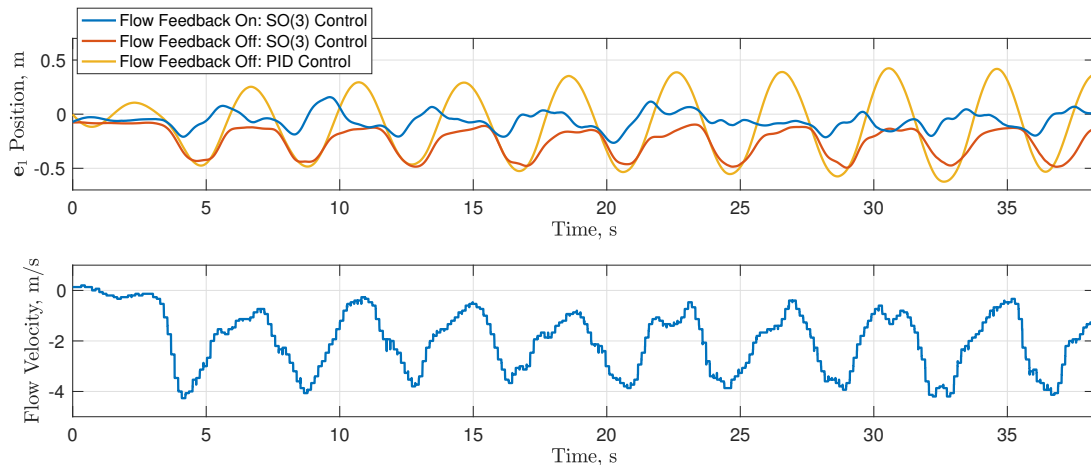


Fig. 6 Experimental quadrotor e_1 position error in response to 2 s duration 4 m/s gusts in the $-e_1$ direction. All three controllers use the same outer-loop control, and flow velocity is measured onboard using a custom flow probe.

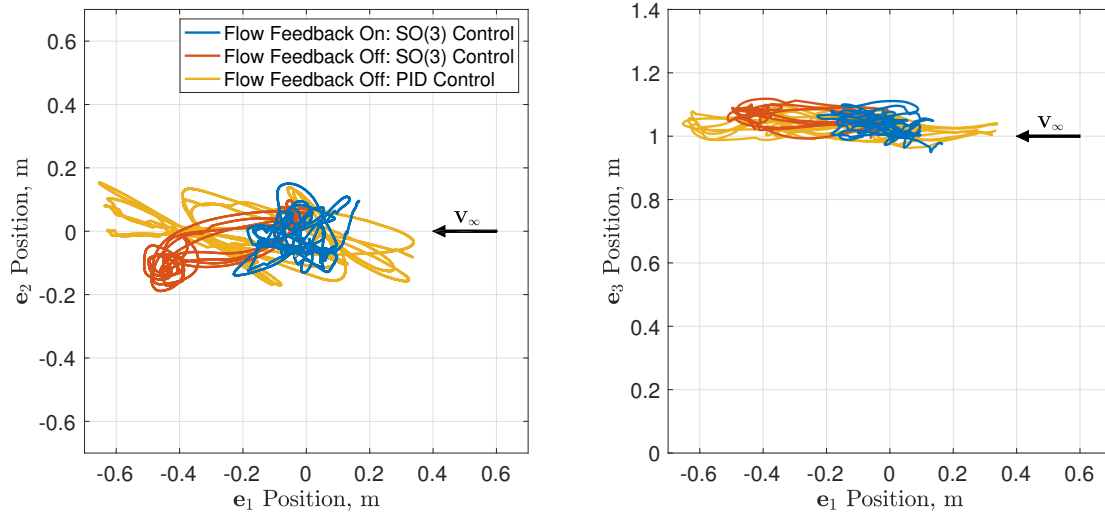


Fig. 7 Experimental quadrotor position response to 5 s duration 4 m/s gusts in the $-e_1$ direction. All three controllers use the same outer-loop control.

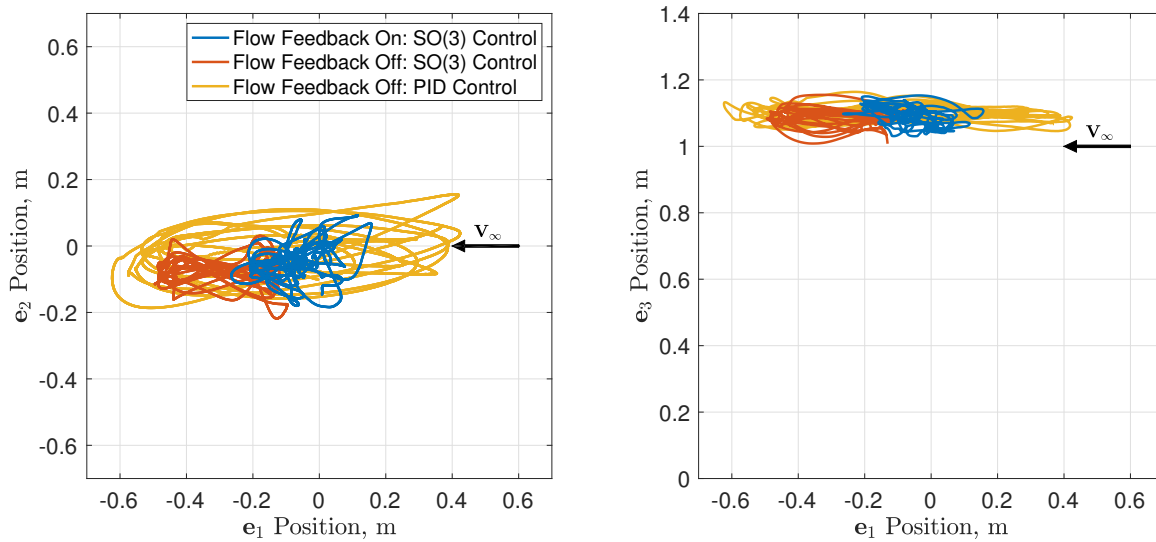


Fig. 8 Experimental quadrotor position response to 2 s duration 4 m/s gusts in the $-e_1$ direction. All three controllers use the same outer-loop control.

For both flow periods, Figs. 5 through 8 show improvement between the PID controller and the $SO(3)$ controller without flow feedback, and additional improvement when flow sensing is added to the $SO(3)$ controller. Both the PID and $SO(3)$ controller without flow feedback show a similar initial error. The PID controller begins moving closer to the desired position until the gust ceases, at which point the integral feedback in the inner loop leads to overshoot. In the 2 second gusts, the PID controller enters a resonant response and error slowly grows as the test progresses, showing higher susceptibility to repeated gusts. The $SO(3)$ controller without flow feedback shows very consistent behavior, returning to the desired position quickly when no wind is present and maintaining a tight offset during each gust. This behavior is shown in the 5 second gusts in Fig. 7 with the position making two tight circles with and without wind. With flow feedback, the quadrotor is able to respond directly to the wind, and there is improvement throughout the tests, with a reduction in initial error and limited overshoot when the gust stops. All controllers hold e_2 and e_3 position well throughout both sets of tests, though we do see slightly more movement in the e_2 direction for $SO(3)$ control with flow feedback as compared to $SO(3)$ without flow feedback as the flow feedback controller responds to measurements and sensor noise in the left-right flow sensor.

VI. Conclusion

This paper describes quadrotor dynamics in wind, augmenting the model with aerodynamic moment and drag terms, which are addressed through flow sensing and feedback control. The controller is built on the Lie group $SE(3)$, and uses variable gains to address motor saturation. Experiments are performed using motion capture feedback for outer-loop position-control and an onboard flight controller that provides attitude feedback. Tests utilize a gust-generation system consisting of fans behind remotely operated blinds, which are opened and closed in a square wave pattern to produce gusts. Results show the benefits of adding flow feedback compared to the same controller without flow feedback as well as the stock PID controller in the Cleanflight firmware. Ongoing work includes flow-feedback validation in outdoor flight as well as development of flow-aware linear controllers.

VII. Acknowledgments

This work was supported by the University of Maryland Vertical Lift Rotorcraft Center of Excellence Army Grant No. W911W6-17-2-0004.

References

- [1] Anderson, C., “10 breakthrough technologies: Agricultural drones,” *MIT Technology Review*, Vol. 117, No. 3, 2014, pp. 58–60.
- [2] Hutson, M., “Hurricanes show why drones are the future of disaster relief,” *NBC MACH*, 2017.
- [3] Gremillion, G. M., and Humbert, J. S., “Disturbance rejection with distributed acceleration sensing for small unmanned aircraft systems,” *AIAA Journal*, Vol. 54, No. 8, 2016, pp. 2233–2246.
- [4] Yeo, D., Sydney, N., and Paley, D., “Onboard flow sensing for downwash detection and avoidance on small quadrotor helicopters,” *Paper AIAA 2015-1769, AIAA Guidance, Navigation, and Control Conference, AIAA SciTech Forum*, 2015, pp. 1–12.
- [5] Sanket, N. J., Singh, C. D., Ganguly, K., Fermüller, C., and Aloimonos, Y., “GapFlyt: Active vision based minimalist structure-less gap detection for quadrotor flight,” *IEEE Robotics and Automation Letters*, Vol. 3, No. 4, 2018, pp. 2799–2806.
- [6] Lupashin, S., Schöllig, A., Sherback, M., and D’Andrea, R., “A simple learning strategy for high-speed quadcopter multi-flips,” *IEEE International Conference Robotics and Automation*, Anchorage, AK, 2010, pp. 1642–1648.
- [7] Goodarzi, F., Lee, D., and Lee, T., “Geometric adaptive tracking control of a quadrotor unmanned aerial vehicle on $SE(3)$ for agile maneuvers,” *Journal of Dynamic Systems, Measurement, and Control*, Vol. 137, No. 9, 2015, pp. 1–12.
- [8] Lanzon, A., Freddi, A., and Longhi, S., “Flight control of a quadrotor vehicle subsequent to a rotor failure,” *Journal of Guidance, Control, and Dynamics*, Vol. 37, No. 2, 2014, pp. 580–591.
- [9] Lee, T., “Geometric control of quadrotor UAVs transporting a cable-suspended rigid body,” *IEEE Transactions on Control Systems Technology*, Vol. 26, No. 1, 2018, pp. 255–264.
- [10] Pereira, P. O., and Dimarogonas, D. V., “Control framework for slung load transportation with two aerial vehicles,” *IEEE Conference on Decision and Control*, Melbourne, Australia, 2018, pp. 4254–4259.

- [11] Leishman, J. G., *Principles of Helicopter Aerodynamics*, 2nd ed., Cambridge University Press, New York, NY, 2006.
- [12] Mellinger, D., and Kumar, V., “Minimum snap trajectory generation and control for quadrotors,” *IEEE International Conference Robotics and Automation*, Shanghai, China, 2011, pp. 2520–2525.
- [13] Cutler, M., and How, J. P., “Analysis and control of a variable-pitch quadrotor for agile flight,” *Journal of Dynamic Systems, Measurement, and Control*, Vol. 137, No. 10, 2015, pp. 1–14.
- [14] Kun, D. W., and Hwang, I., “Linear matrix inequality-based nonlinear adaptive robust control of quadrotor,” *Journal of Guidance, Control, and Dynamics*, Vol. 39, No. 5, 2015, pp. 1–13.
- [15] Yeo, D. W., Sydney, N., and Paley, D. A., “Onboard flow sensing for multi-rotor pitch control in wind,” *Journal of Guidance, Control, and Dynamics*, Vol. 41, No. 5, 2018, pp. 1193–1198.
- [16] Craig, W., Passe, B. E., Yeo, D., and Paley, D. A., “Geometric attitude control of a quadrotor in wind with flow sensing and thrust constraints,” *Submitted to IEEE Transactions on Control Systems Technology*, 2018.
- [17] Lee, T., Leok, M., and Mcclamroch, N. H., “Geometric tracking control of a quadrotor UAV on SE(3),” *IEEE Conference on Decision and Control*, Atlanta, GA, 2010, pp. 5420–5425.
- [18] Cao, N., and Lynch, A. F., “Inner-outer loop control for quadrotor UAVs with input and state constraints,” *IEEE Transactions on Control Systems Technology*, Vol. 24, No. 5, 2016, pp. 1797–1804.
- [19] Cutler, M., and How, J. P., “Actuator constrained trajectory generation and control for variable-pitch quadrotors,” *AIAA Guidance, Navigation, and Control Conference*, Minneapolis, MN, 2012, pp. 1–15.
- [20] Lee, T., Leok, M., and Mcclamroch, N. H., “Nonlinear robust tracking control of a quadrotor UAV on SE(3),” *Asian Journal of Control*, Vol. 15, No. 2, 2013, pp. 391–408.
- [21] Dydek, Z. T., Annaswamy, A. M., and Lavretsky, E., “Adaptive control of quadrotor UAVs: A design trade study with flight evaluations,” *IEEE Transactions on Control Systems Technology*, Vol. 21, No. 4, 2013, pp. 1400–1406.
- [22] Alexis, K., Nikolakopoulos, G., and Tzes, A., “Constrained-control of a quadrotor helicopter for trajectory tracking under wind-gust disturbances,” *IEEE Mediterranean Electrotechnical Conference*, Valletta, Malta, 2010, pp. 1411–1416.
- [23] Roza, A., and Maggiore, M., “A class of position controllers for underactuated VTOL vehicles,” *IEEE Transactions on Automatic Control*, Vol. 59, No. 9, 2014, pp. 2580–2585.
- [24] Teel, A. R., “Global stabilization and restricted tracking for multiple integrators with bounded controls,” *Systems and Control Letters*, Vol. 18, No. 3, 1992, pp. 165–171.
- [25] Pappas, G., Lygeros, J., and Godbole, D., “Stabilization and tracking of feedback linearizable systems under input constraints,” *IEEE Conference on Decision and Control*, New Orleans, LA, 1995, pp. 1–34.
- [26] Craig, W., Yeo, D., and Paley, D. A., “Dynamics of a rotor-pendulum with a small, stiff propeller in wind,” *ASME Dynamic Systems and Controls Conference*, Minneapolis, MN, 2016, pp. 1–10.
- [27] Bullo, F., and Lewis, A. D., *Geometric Control of Mechanical Systems*, Springer, New York, NY, 2005.
- [28] Craig, W., and Paley, D. A., “Geometric control of quadrotor attitude in wind with flow sensing and thrust constraints,” *ASME Dynamic Systems and Controls Conference*, Tysons, VA, 2017, pp. 1–8.